J Appl Physiol 120: 537–545, 2016.
First published December 17, 2015; doi:10.1152/japplphysiol.00245.2015.

Regional specific modulation of the glycocalyx and smooth muscle cell contractile apparatus in conduit arteries of tail-suspended rats

Hongyan Kang, Yubo Fan, Ping Zhao, Changhui Ren, Zhenze Wang, and Xiaoyan Deng

Key Laboratory for Biomechanics and Mechanobiology of Ministry of Education, School of Biological Science and Medical Engineering, Beihang University, Beijing, China

Submitted 23 March 2015; accepted in final form 16 December 2015

Kang H, Fan Y, Zhao P, Ren C, Wang Z, Deng X. Regional specific modulation of the glycocalyx and smooth muscle cell contractile apparatus in conduit arteries of tail-suspended rats. *J Appl Physiol* 120: 537–545, 2016. First published December 17, 2015; doi:10.1152/japplphysiol.00245.2015.—The glycocalyx is a key mechanosensor on the surfaces of vascular cells (endothelial cells and smooth muscle cells), and recently, we reported that the redistribution of the hemodynamic factors in tail-suspended (TS) hindlimb-unloaded rats induces the dimensional adaptation of the endothelial glycocalyx in a regional-dependent manner. In the present study, we investigated the coverage and gene expression of the glycocalyx and its possible relationship with smooth muscle contractility in the conduit arteries from the TS rats. The coverage of the glycocalyx, determined by the area analysis of the fluorescein isothiocyanate-labeled wheat germ agglutinin (WGA-FITC) staining to the cryosections of rat vessels, showed a 27.2% increase in the common carotid artery, a 13.3 and 8.0% decrease in the corresponding abdominal aorta and the femoral artery after 3 wk of tail suspension. The relative mRNA levels of syndecan-2, 3, 4, glypican-1, smooth muscle protein 22 (SM22), smoothelin (SMTN), and calponin were enhanced to 1.40, 1.53, 1.70, 1.90, 2.93, 2.30, and 5.23-fold, respectively, in the common carotid artery of the TS rat. However, both glycocalyx-related genes and smooth muscle contractile apparatus were totally or partially downregulated in the abdominal aorta and femoral artery of the TS rat. A linear positive correlation between the normalized coverage of glycocalyx and normalized mRNA levels of SM22, SMTN, and calponin exists. These results suggest the regional-dependent adaptation of the glycocalyx in simulated microgravity condition, which may affect its mechanotransduction of shear stress to regulate the contractility of the smooth muscle, finally contributing to postspaceflight orthostatic intolerance.

glycocalyx; smooth muscle contractile apparatus; vascular remodeling; orthostatic intolerance; tail-suspended rats

ASTRONAUTS EXPOSED TO MICROGRAVITY often experience postflight orthostatic intolerance on return to the gravity of Earth (16), and its symptoms experienced during standing include increased heart rate, orthostatic hypotension, and frank syncope (28). These alterations of orthostatic stability can delay return to normal upright activities from hours to days and adversely affect the safety, well-being, and performances of astronauts on return to Earth (33). Even after several decades of investigation, mechanisms accounting for orthostatic intolerance, including hypovolemia, cardiovascular structural changes, and alterations in central integration, baroreceptor function, and neurohumoral regulation, remain disputed and multiple (22).

Address for reprint requests and other correspondence: X. Deng, School of Biological Science and Medical Engineering, Beihang Univ., Beijing, China 100191 (e-mail: dengxy1953@buaa.edu.cn).

To investigate this phenomenon on Earth, the tail-suspended hindlimb-unloaded rat has been used extensively to simulate the effect of microgravity (25). This model induces a shift of body fluids toward the head and neck region (39) and postural muscle unloading (27) that occur in microgravity. In addition, the adaptations of the tail-suspended rat, including hypovolemia (26), postural muscle atrophy (27), bone loss (34), and a reduced aerobic capacity (11), are consistent with the observations in spaceflight. Previous studies using tail-suspended hindlimb-unloaded rats strongly suggest that simulated microgravity-induced vascular structural and functional remodeling is anatomically region dependent, and these changes may be one of the key contributors to postspaceflight orthostatic intolerance (6, 9, 40). Adaptations in the upper body arteries, including the increased myogenic tone, enhanced vasoreactivity, hypertrophic remodeling, and endothelial dysfunction, may increase cerebrovascular resistance and contribute to decreased brain blood flow in astronauts when they return to normal gravity conditions (21, 39). On the other hand, remodeling in the lower body arteries, including the decreased myogenic tone, attenuated vasoreactivity, atrophic remodeling, and endothelial dysfunction (36), are likely to result in a diminished ability to raise peripheral resistance in astronauts exposed to orthostatic tests. All these factors operate together to cause orthostatic intolerance when astronauts return to the gravitational environment.

The glycocalyx (GCX) of vascular cells is mainly composed of proteoglycans (syndecans, glypicans, and CD44), with their associated glycosaminoglycans (GAGs) that include heparan sulfate (HS), chondroitin sulfate (CS), and hyaluronic acid (HA), and glycoproteins bearing acidic oligosaccharides with terminal sialic acids (SA) (29). As for the protein backbones of the GAGs, the major carriers of HS and CS are syndecan and glypican family proteins, and HA, on the other hand, is electrostatically bound to the surface glycoprotein CD44 (19). GAG biosynthesis is initiated by the formation of the linkage tetrasaccharide, GlcAβ1-3Galβ1-3Galβ1-4Xylβ1-O-Ser (13), followed by the chain extension steps by the addition of alternating disaccharides catalyzed by exostosin (EXT) 1 and EXT2 (5), or chondroitin synthase (Chsy) (35). As the chain is elongated, sulfate groups are introduced at various positions to make the GAGs highly charged (20). A dynamic equilibrium exists between biosynthesis and shedding of the GAGs induced by enzymes, e.g., heparanase, chondroitinase, and hyaluronidase, or local hemodynamic factors, shear stress in particular (15, 19), continuously affecting the composition and thickness of the GCX.

The physiological importance of the vascular cell glycocalyx (GCX) has been established by functional studies and electron microscopic observations over the past decade. The endothelial

GCX shields the vascular wall from direct exposure to flowing blood, forms a permeability barrier for plasma fluid and macromolecules, limits the adhesion of leukocytes and platelets to the luminal surface, and stimulates NO release by mechanotransduction (7, 8, 14). On the other hand, the smooth muscle cell (SMC) GCX has been reported to play important roles in mechanotransduction of shear stress in two-dimensional (2D) condition where the endothelium has been denuded to modulate cell proliferation, migration, and NO production (17), and function as an interstitial flow sensor in three-dimensional (3D) physiological condition to modulate SMC marker genes (31) and cell motility (32).

Recently, we demonstrated by using confocal microscopy that the redistribution of the hemodynamic factors in tail-suspended hindlimb-unloaded rats induced the dimensional adaptation of the endothelial glycocalyx in a regional-dependent manner, with an approximate 1.66 and 1.64-fold increase in the common carotid artery and the abdominal aorta region and with a 0.79-fold reduction in the femoral artery (18). In the present study, we extended this line of research and focused on the coverage and gene expression of the vascular cell [endothelial cell (EC) and SMC] glycocalyx, and its possible relationship with the expression of smooth muscle contractile apparatus in the conduit arteries from the tail-suspended rats.

MATERIAL AND METHODS

Animal model. Eighteen female Sprague-Dawley rats (specific pathogen free) weighing between 180 and 200 g were provided by National Institutes for Food and Drug Control in China and divided into two groups: control (body wt: 190.40 ± 2.17, $n = 9$) and TS group (body wt: 191.90 ± 2.49, $n = 9$). The number of animals in the present study is consistent with the study about hindlimb unloading effects on muscle flow responses to Ach from Woodman et al. (37). The protocol of tail suspension was supplied by Sun et al. (34) and approved by the Animal Care Committee of Beihang University. In brief, the rat tails were attached to a plastic bar mounted on the top of the cage (30 × 30 × 50 cm) by tape and maintained in about −30° head down-tilt position with their hind limbs unloading. The control rats were kept in the regular cage without tail suspension. All animals were fed by a standard lab chow and kept in a room maintained at 25 ± 2°C on a 12:12 h light/dark cycle for 21 days. The bone mineral density of femurs and tibias from the tail-suspended rats were significantly reduced compared with the control rats, as reported in our previous study (18), verifying the effectiveness of the tail-suspended rat model.

Perfusion and vessel isolation. After anesthetizing with pentobarbital sodium at a dosage of 45 mg/kg, the heart and thoracic aorta were exposed by opening the chest and cutting of the ribs. The left ventricle was located and cannulated, and the perfusion was started with 1% BSA containing 5 IU/ml heparin at 5 ml/min under a pressure of 80 mmHg. Meanwhile, the inferior vena cava was cut to create an outflow. When the blood was completely washed away, the perfusion medium was changed to 2% paraformaldehyde solution, and perfusion continued for another 5 min. Then the arteries from the abdominal, left common carotid, and the left femoral were excised and embedded in Tissue-Tek optimum cutting temperature (OCT, Sakura Finetek USA, Torrance, CA) medium and frozen quickly on dry ice mixed with methanol bath. Arteries used for RNA extraction were washed with sterile PBS only. After getting rid of the collective tissue and the adventitia, the arteries were excised carefully and frozen as soon as possible.

RNA extraction and quantitative PCR. Total RNA was extracted from the common carotid artery (≈11 mg), abdominal aorta (≈43 mg), and the femoral artery (≈8 mg) of the control and tail-suspended rats by using TRNzol reagent (Invitrogen, Camarillo, CA). The amount of total RNA from each sample was quantified with a NanoDrop 2000 spectrophotometer (Thermo Scientific, Wilmington, DE). Genomic DNA elimination was performed by incubating 1 μg total RNA of each sample with gDNA eraser at 42°C for 2 min. RNA was subsequently reverse transcribed with a PrimeScriptTM RT reagent Kit (Takara Bio, Otsu, Japan) and real-time PCR was performed on iQ5 Multicolor Real-Time PCR Detection System (Bio-Rad, Hercules, CA) with a SYBR Green master mix (Takara Bio, Otsu, Japan). Specific gene primers employed for quantitative PCR are listed in Table 1. The amplification efficiency of each primer was confirmed by melting curve analysis. Triplicates of each sample from control and tail-suspended rats were run in the same experiment. Quantification of the relative changes in mRNA levels between control and TS groups was performed by the delta delta threshold cycle ($\Delta\Delta C_t$) method. ΔC_t was calculated by subtracting the C_t value of the target gene from the C_t value of the internal reference gene GAPDH. $\Delta\Delta C_t$ was obtained by subtracting the ΔC_t value of the TS group from the ΔC_t value of the control group in the same experiment. Fold change was then calculated as $2^{-\Delta\Delta C_t}$. Data from four couples of control and tail-suspended rats were used to analyze the relative expression level for each gene.

Immunofluorescence staining and confocal microscopy. The protocol of artery glycocalyx staining with fluorescein isothiocyanate-labeled wheat germ agglutinin (WGA-FITC, Sigma Aldrich, St.

Table 1. *Specific gene primers used for real-time PCR*

Gene	Accession No.	Sense	Antisense	Location	Size
Syndecan-2	AA925627.1	TTCACTGTTTTGCACAGTTA	CTTCCAAAGCTGCACAATGC	142–220	79
Syndecan-3	U52825.1	CACCTCCTCCCAGGGAAAG	ACGCTAGAGTGGCCTCCCTTA	1925–1994	70
Syndecan-4	NM_012649.2	TGTTTTTGACCCTGGCCCTT	ATCCCGCTACCCCCTACATT	1615–1711	97
Glypican-1	NM_030828.1	ACAATTTAATCATTGGCAGTGTGCATATGTG	AGCCTCAATCTTTAGCTGTGAGTGTGTCCTTGTTG	1150–1245	96
CD44	NM_012924.2	GCCAGTGACAGGTTCCATTCA	AGGATCTAGTAGCCTCTGGAAAAGG	22–92	71
Chsy1	NM_001106268.1	GGTCGAGCTGATGCGAGATT	GTGCTCTCGAAAACCCTCCA	1739–1824	86
EXT1	NM_001130540.1	AGTCCCAGCCAGTGTTGAAG	GTGTTTGGCTGGTAGAGGCT	1598–1701	104
Hyaluronidase-1	AB100600.1	TCGGACCCTTTATCCTGAAC	TTCTTACACCACTCTCCACTC	1076–1337	262
Hyaluronidase-2	AF034218.1	TCAGTGTACGCTTCAAGTATGGA	GACTGAGGTGCAAGAAGGTACTG	1105–1285	181
Chondroitinase	NM_001047851.1	TGTGCTACTGCTCATGGACG	AGCACAAAGGGTTGGCAGAA	102–241	140
SM-MHC	NM_001170600.1	AAGCAGCTCAAGAGGCAG	AAGGAACAAATGAAGCCTCGTT	5786–5963	178
α-SMA	NM_031004.2	GATCACCATCGGGAATGAACGC	CTTAGAAGCATTTGCGGTGGAC	804–1192	389
SM22	NM_031549.2	TGTTCCAGACTGTTGACCTC	GTGATACCTCAAAGCTGTCC	384–752	369
SMTN	NM_001013049.2	TCGGAGTGCTGGTGAATAC	CCCTGTTTCTCTTCCTCTGG	514–711	198
Calponin	NM_031747.1	ACAAAAGGAAACAAAGTCAAT	GGGCAGCCCATACACCGTCAT	463–858	396
GAPDH	NM_017008.4	GCTCTCTGCTCCTCCCTGTTCT	CAGGCGTCCGATACGGCCAAA	4–120	117

Louis, MO) was described sophisticatedly in our previous study. In brief, the frozen vessels embedded in OCT were first cut into 6-μm slices by using a Leica CM1950 cut machine (Leica Biosystems, Shanghai, China) and mounted on superfrost plus microscope slides (Thermo Scientific, Portsmouth, NH). After exposing to air dry overnight, the slides were then postfixed in 4% paraformaldehyde solution for 10 min. Antigen retrieval was performed by warming the slides in 0.01 M sodium citrate to 92-95°C for 15 min. After cooling for 30 min, the slides were washed in PBS and treated with 1% H_2O_2 for 30 min, then incubated with WGA-FITC at 5 μg/ml for 4 hr in dark. Thereafter, the slides were mounted with Antifade mounting medium with DAPI (HelixGen, Guangzhou, China) and imaged under a Leica TCS SPE confocal microscope (Leica Microsystems, Wetzlar, Germany). A ×40 oil objective lens was applied and the field of view (FOV) was about 275 × 275 μm with a 1,024 × 1,024 pixel solution. For the common carotid artery and the abdominal aorta, three FOVs were chosen for each slice and three to five slices were collected for each vessel. For the femoral artery, on the other hand, two FOVs were imaged for each slice and four to five slices were chosen for each vessel. Vessels from five couples of control and tail-suspended rats were used to analyze the coverage of the glycocalyx.

Image analysis. Images were analyzed with Image J software (National Institutes of Health, Bethesda, MD) that is free and available from the website. To quantify the coverage of the GCX, images were turned to 8-bit type by performing the split channels as shown in Fig. 1, *A–C*. For a given FOV of WGA-FITC staining, the intima and media were selected with the polygon selections tool and outlined as the region of interest (ROI) as designated in Fig. 1*D*. Regions outside the ROI were cleared (Fig. 1*E*) and the ROI was then threshold automatically (Fig. 1*F*). The coverage of the glycocalyx was defined as the area of the WGA-FITC positive staining divided by the total area of the ROI and presented as a percent. It should be noted that only well-stained areas of one slice with clearly labeled GCX and low background was selected when calculating the coverage of GCX. Areas with high background or low contrast were excluded since it would lower the result of the calculation. Although the brightness of the WGA-FITC staining cannot affect the calculation of the GCX coverage significantly (unpublished data), all images were still obtained at the same intensity of excitation.

Statistics. The coverage of GCX and the relative mRNA levels of smooth muscle contractile apparatus in common carotid artery, abdominal aorta, and femoral artery were normalized by each value of the control rats. A Kolmogorov-Smirnov test with a Dallal-Wilkinson-Lilliefor *P* value was performed to test if the values came from a Gaussian distribution. Correlations were evaluated between normalized coverage of GCX and normalized mRNA levels of smooth muscle contractile apparatus by using the nonparametric Spearman correlation coefficient.

Data are presented as means ± SE. Differences were assessed by using unpaired Student's *t*-test with $P < 0.05$ considered significant.

RESULTS

The coverage of the glycocalyx quantification. WGA-FITC binds N-acetylated glucosamine residues in HS, HA, and SA, so it labeled the component of glycocalyx from the intima to adventitia except for the elastic fiber, as shown in Fig. 2. The arrowheads denote the endothelial cells and arrows show the internal elastic lamina. The coverage of the glycocalyx, presented as a percent of the WGA-FITC positive staining area divided by the total area of the vessel (adventitia excluded), showed an approximate 27.2% increase in the common carotid artery (TS 78.8 ± 2.8% vs. control 51.6 ± 1.6%, $P < 0.01$), a 13.3% decrease in the abdominal aorta (TS 32.4 ± 2.3% vs. control 45.7 ± 3.8%, $P < 0.01$), and a 8.0% decrease in the femoral artery (TS 26.6 ± 2.5% vs. control 34.6 ± 2.3%, $P < 0.05$) of the tail-suspended rats (Fig. 3). These results suggest the total amount of the glycocalyx would be modulated by simulated microgravity in a regional-dependent manner.

Expression of glycocalyx-related genes. To evaluate the effect of simulated microgravity on the expression of the components of vascular cell glycocalyx, we quantified the mRNA levels

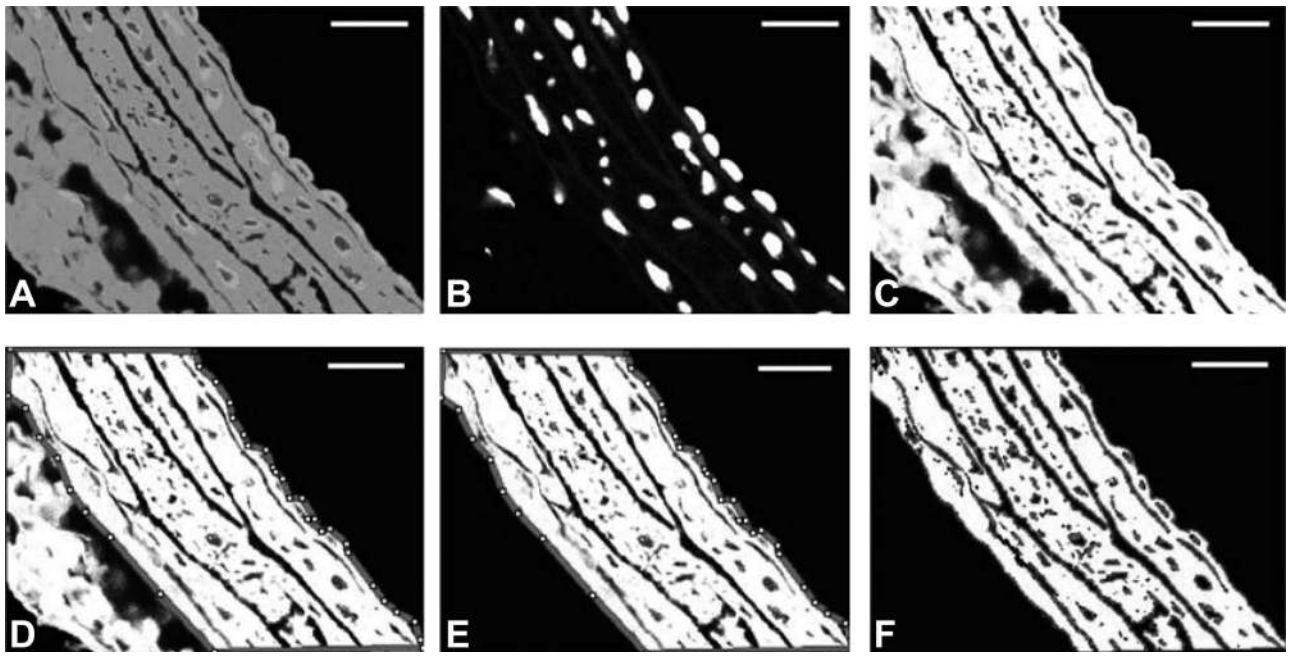

Fig. 1. Instructions for image analysis. *A–C*: the original images (*A*) were split into two 8-bit-type images with DAPI (*B*) and fluorescein isothiocyanate-labeled wheat germ agglutinin (WGA-FITC) (*C*) staining, respectively. *D*: the intima and media of one slice with WGA-FITC staining were selected and outlined. *E*: the outside of the selected area (*D*) was cleared. *F*: selected area was the threshold. Scale bar = 20 μm.

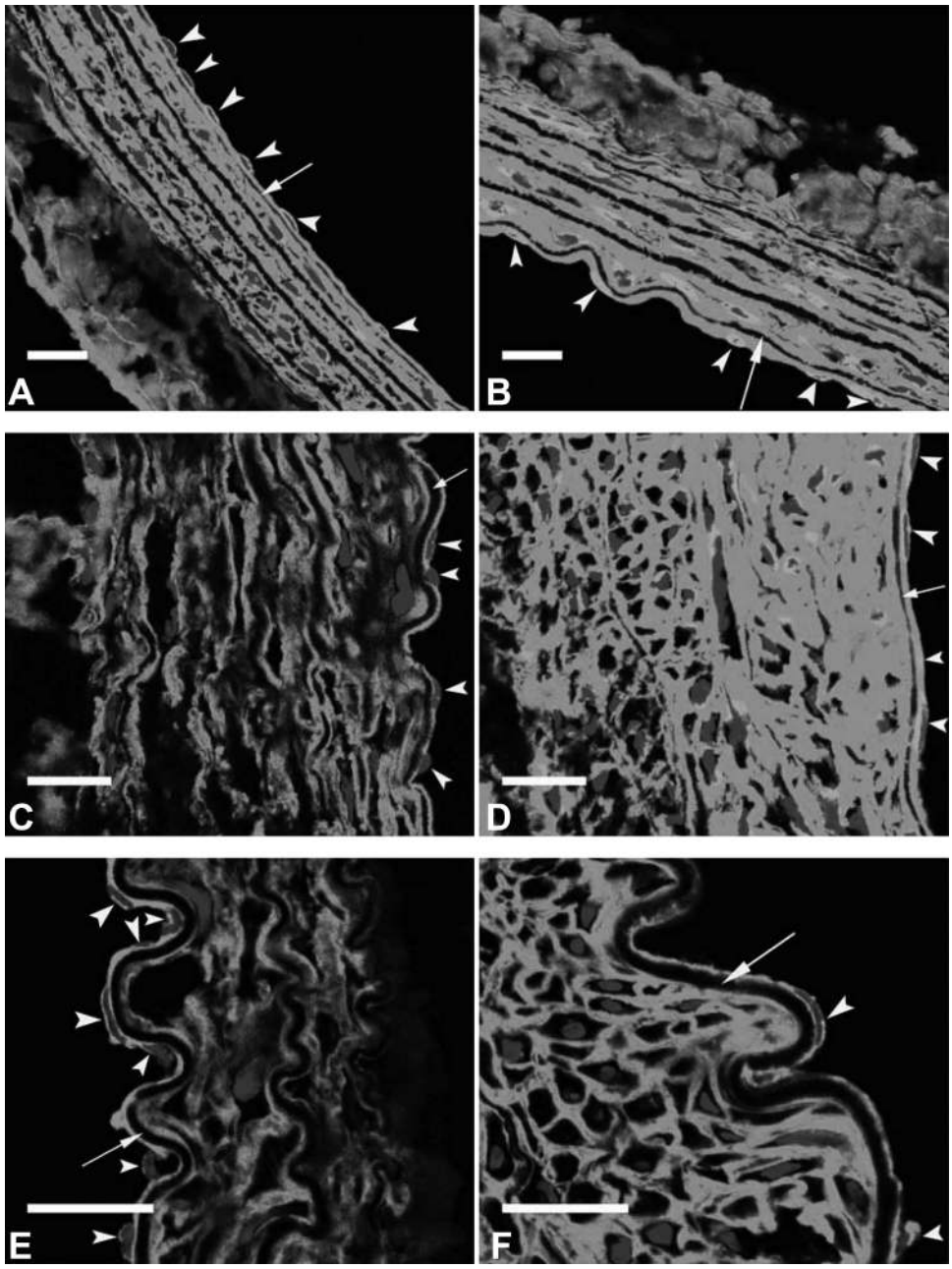

Fig. 2. Representative photographs of the common carotid artery (*A–B*), abdominal aorta (*C–D*), and the femoral artery (*E–F*) stained by DAPI and WGA-FITC from control (*A*, *C*, and *E*) and tail-suspended (*B*, *D*, and *F*) rats. Arrowheads denote the endothelial cells. Arrows show the internal elastic lamina. Scale bar = 20 μm.

of its core protein backbones (syndecan, glypican, and CD44) and the key biosynthesis and degradation enzymes of the GAGs. Samples from one couple of TS and control rats were run side by side with three replicates for each target gene and GAPDH at the same time, and data from four couples of rats were used to calculate the means ± SE. As shown in Fig. 4*A*, the relative mRNA levels of the core protein backbones, including syndecan-2, 3, 4, and glypican-1, show a 1.40 ($P < 0.05$), 1.53 ($P < 0.05$), 1.70 ($P < 0.05$), 1.90-fold ($P < 0.01$) increase in the common carotid artery of the tail-suspended rats with respect to the control group. There were no significant differences of the relative mRNA levels of other genes like CD44, Chsy1, EXT1, hyaluronidase-1, hyaluronidase-2, and chondroitinase between the tail-suspended and control rats ($P > 0.05$). For the abdominal aorta, all target genes were downregulated significantly by the tail suspension of rats, and the relative mRNA levels were ranged from 0.14 to 0.44-fold compared with the control rats (Fig. 4*B*). Moreover, the same downregulation trend was observed in the femoral artery of tail-suspended rats, as shown in Fig. 4*C*. Briefly, relative mRNA levels of syndecan-3 (0.43-fold, $P < 0.01$), glypican-1 (0.19-fold, $P < 0.01$), CD44 (0.75-fold, $P < 0.01$), Chsy1 (0.53-fold, $P < 0.05$), EXT1 (0.57-fold, $P < 0.01$), hyaluronidase-2 (0.44-fold, $P < 0.05$), and chondroitinase (0.38-fold, $P < 0.01$) show significant reduction, while the mRNA levels of syndecan-2, syndecan-4, and hyaluronidase-1 seem not affected by the tail suspension of rats.

Expression of smooth muscle cell contractile apparatus. Smooth muscle cells in normal vessels exhibit a mature contractile apparatus, including smooth muscle myosin heavy

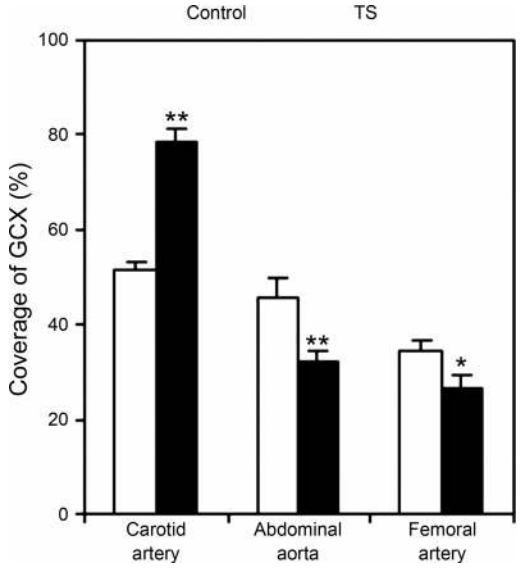

Fig. 3. The coverage of the glycocalyx (GCX) (%) presented as a percent of the WGA-FITC positive staining area divided by the total area of the vessel (adventitia excluded). TS, tail-suspended rats. *$P < 0.05$ vs. control; **$P < 0.01$ vs. control.

chains (SM-MHC), smooth muscle α-actin (α-SMA), smooth muscle protein 22 (SM22), smoothelin (SMTN), and calponin. Relative expression levels of these marker proteins can be used to evaluate the contractility of one vessel in the literature. To exam effect of simulated microgravity on vascular contractility, relative mRNA levels of smooth muscle contractile marker proteins from three different vessels (the common carotid artery, abdominal aorta, and femoral artery) were measured by qRT-PCR. Samples from four couples of control and tail-suspended rats were run at one time for one target gene and GAPDH, and each sample has three replicates for both target gene and GAPDH. As shown in Fig. 5, the tail suspension of rats significantly reduced the relative mRNA levels of all contractile markers, including SM-MHC (0.41-fold, $P < 0.05$), a-SMA (0.24-fold, $P < 0.01$), SM22 (0.16-fold, $P < 0.01$), SMTN (0.40-fold, $P < 0.01$), and calponin (0.18-fold, $P < 0.05$), in the abdominal aorta (Fig. 5*B*) and the relative mRNA level of SMTN (0.23-fold, $P < 0.05$) in the femoral artery (Fig. 5*C*), while upregulated the expressions of SM22, SMTN, and calponin to 2.93 ($P < 0.05$), 2.30 ($P < 0.05$), and 5.23-fold ($P < 0.01$), respectively, in the common carotid artery (Fig. 5*A*).

Correlations evaluation. Results from Kolmogorov-Smirnov normality test showed that the normalized coverage of GCX and normalized mRNA levels of smooth muscle contractile apparatus, including SM-MHC, SM22, SMTN, and calponin, were not from a Gaussian distribution, with a P value < 0.05. Therefore, nonparametric Spearman correlation between the normalized coverage of GCX and normalized mRNA levels of smooth muscle contractile apparatus was performed to compute the correlation coefficients, which are based on ranks, not the actual values. As shown in Fig. 6, the Spearman coefficients (r) for SM-MHC and a-SMA were 0.613 both with a P value > 0.05, which indicates the correlations were not significant. For SM22, SMTN, and calponin, however, the Spearman coefficients were 1.000 ($P = 0.017$), 0.936 ($P = 0.033$), and 1.000 ($P = 0.017$), with a slope of 3.11, 2.50, and 5.99, respectively.

DISCUSSION

Fig. 2 shows the typical WGA-FTIC staining of the glycocalyx (GCX) from the intima to adventitia of one vessel slice, which is consistent with our earlier confocal microscopic observation that WGA-FITC labeled the HS, HA, and SA component of the GAGs from the EC and SMC membrane, extracellular matrix, and cytoplasm (18). This kind of intima to adventitial staining has also been observed by Megens et al. (24) in their two-photon microscopic study of the murine arteries by adding WGA-FITC intra- and extraluminally 30 min before image acquisition in a perfusion chamber. At the cellular level, WGA-FITC labeled both the cell membrane and extracellular matrix. This phenomenon is consistent with the results obtained by Barker et al. (3) in the cultured human endothelial cells. Moreover, the cytoplasmic staining of WGA-FITC may be the intracellular heparin sulfate taken up by cells through endocytosis as reported by Barkefors et al. (2).

Results from Fig. 3 showed that the tail suspension of rats modulated the coverage of the GCX in an anatomic regional-dependent manner, with an approximate 27.2% increase in the common carotid artery and a respective 13.3 and 8.0% decrease in the abdominal aorta and the femoral artery of the tail-suspended rats. This phenomenon was associated with the expression levels of glycocalyx-related genes, including the core protein backbones and the key biosynthesis and degradation enzymes of GAGs, as shown in Fig. 4. Briefly, the significant increase of the relative mRNA levels of syndecan-2, 3, 4 and glypican-1 in the common carotid artery of tail-suspended rats (Fig. 4*A*) suggests more carriers of HS and CS, contributing to the enhanced local coverage of GCX. Accordingly, the downregulation of protein carriers (syndecan-2, 3, 4, glypican-1, and CD44) and biosynthesis enzymes (Chsy1 and EXT1) of GAGs in the abdominal aorta of tail-suspended rats, as shown in Fig. 4*B*, indicates less protein backbones and GAG side chains compared with the control rats. Meanwhile, a less extent of downregulation for the key endogenous degradation enzymes of GAGs, including hyaluronidase-1 (0.44-fold), hyaluronidase-2 (0.36-fold), and chondroitinase (0.19-fold), compared with the biosynthesis enzymes, including Chsy1 (0.17-fold) and EXT1 (0.14-fold), acts together and contributes to the final 13.3% reduction in the local coverage of GCX. In the same way, the downregulated relative mRNA levels of syndecan-3 (0.43-fold), glypican-1 (0.19-fold), CD44 (0.75-fold), Chsy1 (0.53-fold), EXT1 (0.57-fold), hyaluronidase-2 (0.44-fold), and chondroitinase (0.38-fold) in the femoral artery of the tail-suspended rats (Fig. 4*C*), suggesting a reduction in the amount of protein carriers, biosynthases, and degradation enzymes of GAGs, results in a 8.0% decrease of the local coverage of GCX. Collectively, these results, in line with our previous endothelial glycocalyx dimensional study, demonstrated that simulated microgravity could induce arterial glycocalyx remodeling, not only the thickness but also the coverage and the gene expressions, in an anatomic regional-dependent manner.

How does this kind of remodeling of arterial glycocalyx happen? It should be noted that the tail suspension of rat can induce a shift of the body fluid toward its head and neck region, resulting in the redistribution of transmural pressures and flows

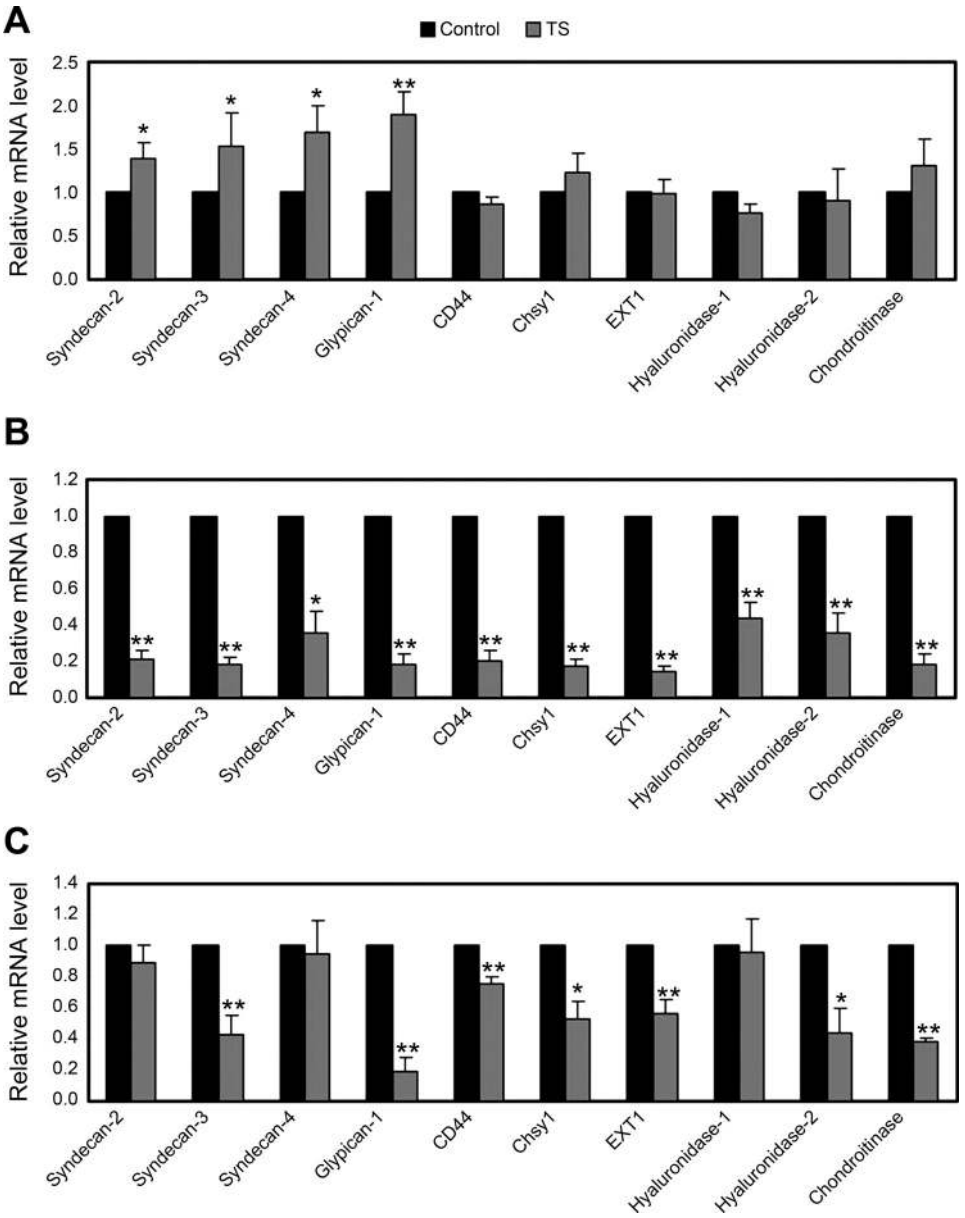

Fig. 4. The relative mRNA levels of glycocalyx-related genes, including its core protein backbones (syndecan-2, 3, 4, glypican-1, and CD44) and the key biosynthesis (Chsy1 and EXT1) and degradation enzymes (hyaluronidase-1, 2 and chondroitinase) of the glycosaminoglycans in the common carotid artery (*A*), abdominal aorta (*B*), and the femoral artery (*C*) of control and TS rats. Samples from one couple of control and TS rats were run side by side with three replicates for each target gene and GAPDH at one experiment. The relative mRNA level was calculated as $2^{-\Delta\Delta Ct}$ for one experiment, and data from four experiments were used to calculate the means ± SE. Chsy: chondroitin synthase. EXT: exostosin. $^{*}P < 0.05$ vs. control; $^{**}P < 0.01$ vs. control.

within and across the arterial vasculature (39). Although direct measurements of the local hemodynamic stress conditions are rare, data from experimental studies have estimated that during tail suspension, the blood flow in the rat abdominal aorta could be reduced by about 23% (10), and the mean blood pressure in its basilar artery would be increased by about 17 mmHg (36) compared with the control standing group. These alterations of local hemodynamic stresses, shear stress in particular, could be some kind of mechanical stimuli that affect the expression of several components of glycocalyx and initiate the local vascular glycocalyx remodeling, as was first reported by Gouverneur et al. (15). They applied a 10-dyn/cm^2 shear stress on human umbilical vein endothelial cells for 24 h and found that fluid shear stress stimulates incorporation of hyaluronan into glycocalyx, contributing to its vasculoprotective effects against proinflammatory and proatherosclerotic stimuli. Very recently, Koo et al. (19) investigated the expression of human endothelial cell glycocalyx components by exposing cells to atherosclerosis-resistant or atherosclerosis-susceptible shear waveforms and found that the expression of glycocalyx components was differentially regulated by distinct hemodynamic environments, which linked the distinct hemodynamic environments to the expression of key components of endothelial glycocalyx directly. Although the effect of transmural pressures on the expression of glycocalyx components has not been revealed, Dull et al. (12) demonstrated a pressure-sensitive mechanotransduction role of the endothelial glycocalyx in modulating the hydraulic conductivity of cultured lung microvascular endothelial cells, suggesting some possible relationships between pressure and the endothelial glycocalyx. In all, these studies have supplied supporting material to explain the observations in the present study that the expression of several components of vascular cell glycocalyx could be modulated by distinct hemodynamic environments induced by the redistribution of body fluid in tail-suspended rats.

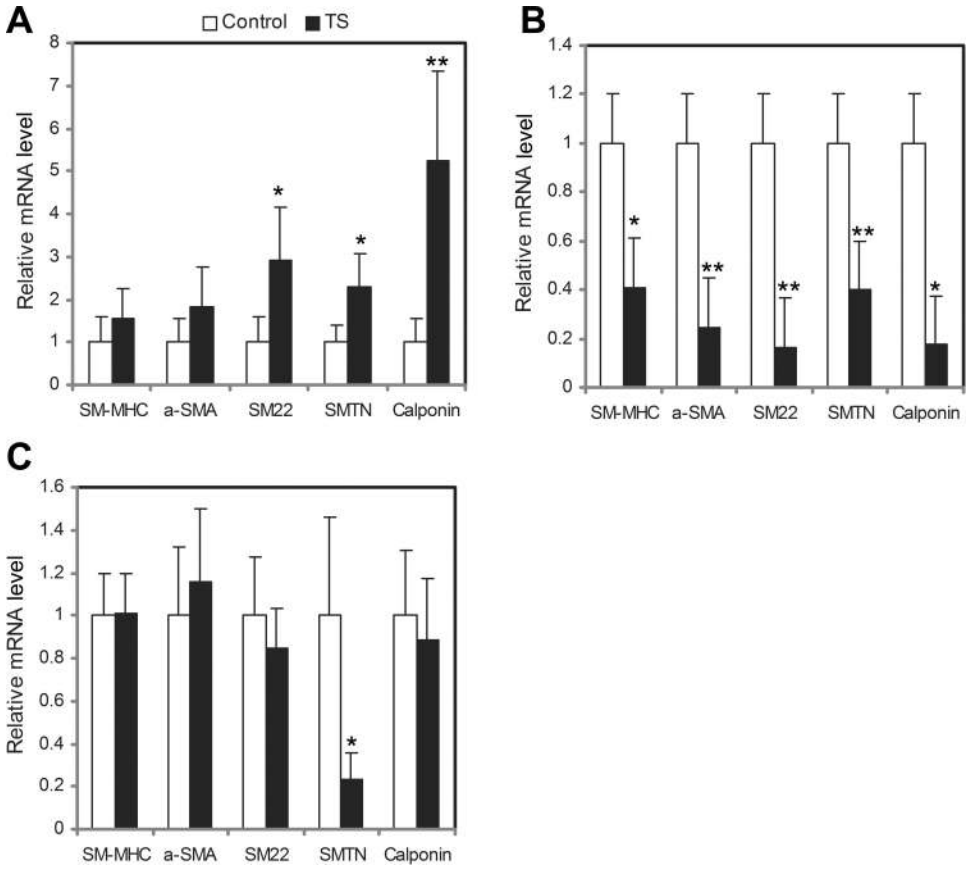

Fig. 5. The relative mRNA levels of smooth muscle contractile apparatus, including SM-MHC, α-SMA, SM22, SMTN, and calponin in the common carotid artery (*A*), abdominal aorta (*B*), and the femoral artery (*C*) of control and TS rats. Samples from four couples of control and tail-suspended rats were run at one time for one target gene and GAPDH, and each sample has three replicates for both target gene and GAPDH. Data from four couples of control and TS rats were used to calculate the means ± SE at one time. SM-MHC, smooth muscle myosin heavy chains; α-SMA, smooth muscle α-actin; SM22, smooth muscle protein 22; SMTN, smoothelin. $*P < 0.05$ vs. control; $**P < 0.01$ vs. control.

SMCs in normal vessels retain remarkable plasticity to transform between "contractile" and "synthetic" phenotypes in response to alterations in local environmental conditions (31), and the relative expression of its contractile apparatus including smooth muscle myosin heavy chains (SM-MHC), smooth muscle α-actin (a-SMA), SM22, smoothelin (SMTN), and calponin (4), combined with calmodulin expression (38) and myosin light-chain kinase activity (39) could be used to evaluate the contractility of one vessel. Results from Fig. 5*B* showed that the 3-wk tail suspension of rats significantly reduced the relative mRNA levels of all contractile markers, including SM-MHC, a-SMA, SM22, SMTN, and calponin, in the abdominal aorta, indicating the decrement in the ability of smooth muscle to generate force. This observation is consistent with the results from the maximal isometric contractile tension measurements that both receptor-mediated and nonreceptor-mediated vasoconstrictor responses of the abdominal aorta decreased significantly after 2 wk (10), 20 days (30), and 4 wk (23) of tail suspension. However, results from Fig. 5, *A* and *C*, showing no significant change of the relative mRNA levels of two main force generation apparatus (SM-MHC and a-SMA) while increased or decreased relative mRNA levels of contractile modulation apparatus (SM22, SMTN, or calponin) in the common carotid and femoral artery of the tail-suspended rats suggest somewhat enhanced or impaired contractility of the smooth muscle. This phenomenon seems contradictory to the results from Purdy et al. (30). They examined the contractility of different conduit arteries of 20-day tail-suspend rats and showed that the tail-suspension treatment of rats decreased the contraction responses to 68 mM KCl and norepinephrine in the common carotid artery but had no significant effect on the femoral artery. The reason for this discrepancy is multiple. In addition to the gender differences of the SD rats (the female rat in our present study vs. male in Purdy's study), the method used to evaluate the contractility of the smooth muscle can directly affect the final results. For example, Purdy et al. measured the length-tension relationship of the vessel ring, which directly indicates the biomechanical properties of one vessel. Our group, on the other hand, measured the relative mRNA levels of smooth muscle contractile apparatus, which reflects the biochemical property of one vessel more properly. Moreover, it is hard to make a conclusion of the contractility adaptation of one vessel only from the alterations in the mRNA levels of SM22, SMTN, or calponin since they are the contractile regulator not the main force generation apparatus (4).

Correlation evaluation in the present study was based on the normalized values of GCX coverage and the relative mRNA levels of smooth muscle contractile apparatus by the relative values of the control rats, which can eliminate the baseline differences in the common carotid artery, abdominal aorta, and the femoral artery. Although the data used to compute the correlation coefficients is not big, it indeed shows a significant linear positive correlation between the normalized coverage of GCX and normalized mRNA levels of smooth muscle contractile regulatory apparatus (SM22, SMTN, and calponin), which is consistent with the observations from cultured smooth muscle cells (1, 31). Shi et al. (31) exposed vascular smooth muscle cells to 8 dyn/cm^2 laminar shear stress (2D) and interstitial flow (3D) for different times and showed that the component of the glycocalyx (HSPG) mediated ERK1/2 activation is an

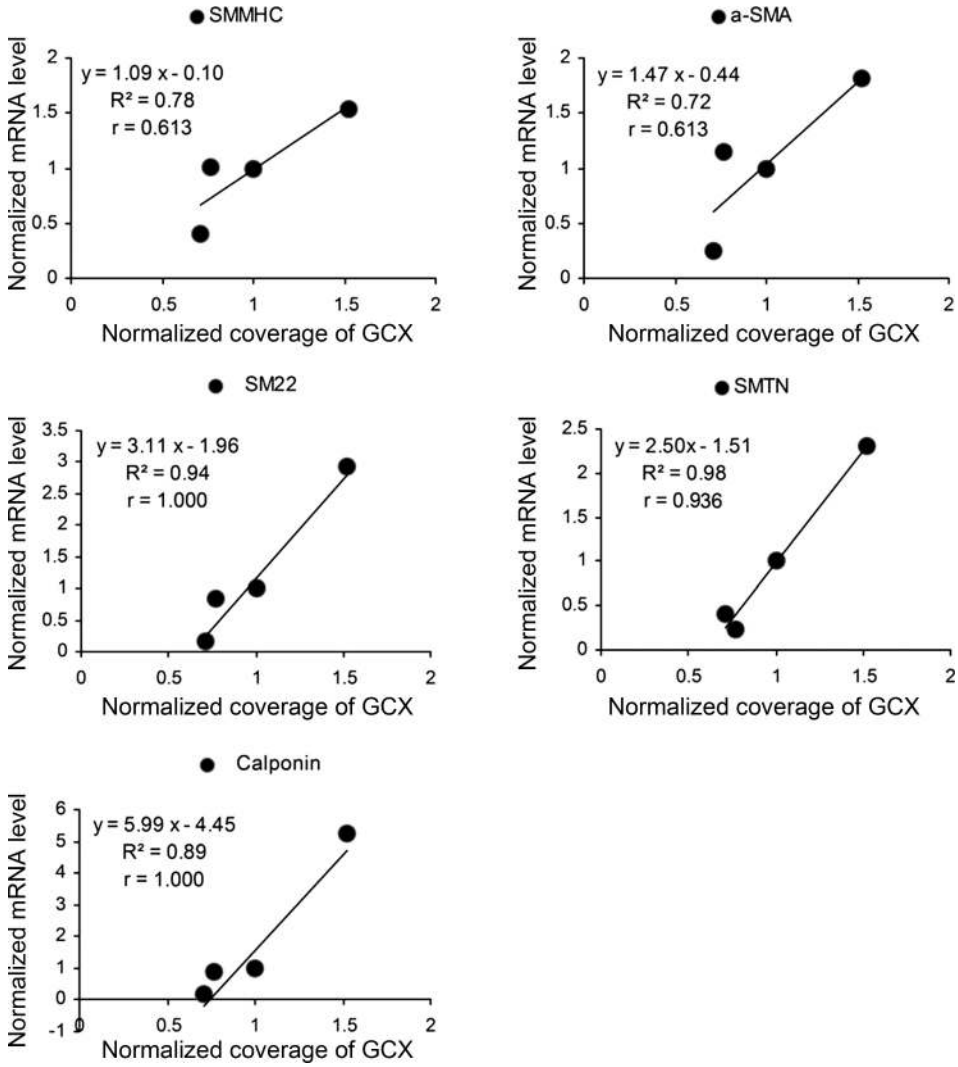

Fig. 6. Correlations evaluation between the normalized coverage of GCX and normalized mRNA levels of smooth muscle contractile apparatus. Spearman coefficients (r) for SM-MHC, α-SMA, SM22, SMTN, and calponin were 0.613 ($P > 0.05$), 0.613 ($P > 0.05$), 1.000 ($P = 0.017$), 0.936 ($P = 0.033$), and 1.000 ($P = 0.017$), respectively.

important pathway modulating SMC marker gene expression. In addition, Ainslie et al. (1) found that when the glycocalyx of the SMC was partially degraded by enzyme, the contraction response to increase in shear stress was significantly inhibited.

In conclusion, we found that 3-wk tail suspension of rats increases the coverage of GCX and the relative mRNA levels of the core protein backbones of the glycosaminoglycans (GAGs) and the SMC contractile regulatory apparatus (SM22, SMTN, and calponin) in the common carotid artery, and decreases the coverage of GCX and the relative mRNA levels of all glycocalyx-related genes and smooth muscle contractile apparatus in the abdominal aorta. For the rat femoral artery, the coverage of GCX is reduced, and the glycocalyx-related genes and smooth muscle contractile apparatus were partially down-regulated after 3 wk of tail suspension. A significant linear positive correlation between the normalized coverage of GCX and normalized mRNA levels of smooth muscle contractile regulatory apparatus (SM22, SMTN, and calponin) exists. Collectively, these results suggest that the redistribution of hemodynamic factors across the arterial vasculature in the simulated microgravity condition regulates the vascular cell glycocalyx, not only the thickness but also the coverage and the gene expression, in a regional-dependent manner, which may affect its mechanotransduction of shear stress to regulate the contractility of the smooth muscle, finally contributing to postspaceflight orthostatic intolerance.

ACKNOWLEDGMENTS

The authors thank Dr. Eno E Ebong, Dr. Limary M. Cancel, and Wan-Yi Yen from the City College of New York for providing help on the glycocalyx staining, and Dr. Lianwen Sun and Yunfei Huang for providing help on the tail suspension of rats.

GRANTS

This work was supported by Grants-in-Aid from the National Natural Science Research Foundation of China (No. 31500763, 11332003, and 11421202) and the 111 Project (B13003) and Special Fund for Excellent Doctor Degree Dissertation of Beijing (20131000601).

DISCLOSURES

No conflicts of interest, financial or otherwise, are declared by the author(s).

AUTHOR CONTRIBUTIONS

H.K., P.Z., and C.R. performed experiments; H.K. analyzed data; H.K. drafted manuscript; H.K., Y.F., P.Z., C.R., Z.W., and X.D. approved final version of manuscript; Y.F. and X.D. conception and design of research; Z.W. prepared figures; X.D. edited and revised manuscript.

REFERENCES

1. **Ainslie KM, Garanich JS, Dull RO, Tarbell JM.** Vascular smooth muscle cell glycocalyx influences shear stress-mediated contractile response. *J Appl Physiol (1985)* 98: 242–249, 2005.
2. **Barkefors I, Aidun CK, Egertsdotter EMU.** Effect of fluid shear stress on endocytosis of heparan sulfate and low-density lipoproteins. *J Biomed Biotechnol* 2007: 65136, 2007.
3. **Barker AL, Konopatskaya O, Neal CR, Macpherson JV, Whatmore JL, Winlove CP, Unwin PR, Shore AC.** Observation and characterisation of the glycocalyx of viable human endothelial cells using confocal laser scanning microscopy. *Phys Chem Chem Phys* 6: 1006–1011, 2004.
4. **Beamish JA, He P, Kottke-Marchant K, Marchant RE.** Molecular regulation of contractile smooth muscle cell phenotype: implications for vascular tissue engineering. *Tissue Eng Part B Rev* 16: 467–491, 2010.
5. **Busse M, Feta A, Presto J, Wilen M, Gronning M, Kjellen L, Kusche-Gullberg M.** Contribution of EXT1, EXT2, and EXTL3 to heparan sulfate chain elongation. *J Biol Chem* 282: 32802–32810, 2007.
6. **Cheng JH, Zhang LF, Gao F, Bai YG, Boscolo M, Huang XF, Zhang X.** Mechanics and composition of middle cerebral arteries from simulated microgravity rats with and without 1-h/d -Gx gravitation. *PLoS One* 9: e97737, 2014.
7. **Constantinescu AA, Vink H, Spaan JA.** Endothelial cell glycocalyx modulates immobilization of leukocytes at the endothelial surface. *Arterioscler Thromb Vasc Biol* 23: 1541–1547, 2003.
8. **Curry FE.** Determinants of capillary permeability: a review of mechanisms based on single capillary studies in the frog. *Circ Res* 59: 367–380, 1986.
9. **Delp MD, Colleran PN, Wilkerson MK, McCurdy MR, Muller-Delp J.** Structural and functional remodeling of skeletal muscle microvasculature is induced by simulated microgravity. *Am J Physiol Heart Circ Physiol* 278: H1866–H1873, 2000.
10. **Delp MD, Holder-Binkley T, Laughlin MH, Hasser EM.** Vasoconstrictor properties of rat aorta are diminished by hindlimb unweighting. *J Appl Physiol (1985)* 75: 2620–2628, 1993.
11. **Desplanches D, Mayet MH, Sempore B, Frutoso J, Flandrois R.** Effect of spontaneous recovery or retraining after hindlimb suspension on aerobic capacity. *J Appl Physiol (1985)* 63: 1739–1743, 1987.
12. **Dull RO, Mecham I, McJames S.** Heparan sulfates mediate pressure-induced increase in lung endothelial hydraulic conductivity via nitric oxide/reactive oxygen species. *Am J Physiol Lung Cell Mol Physiol* 292: L1452–L1458, 2007.
13. **Esko JD, Lindahl U.** Molecular diversity of heparan sulfate. *J Clin Invest* 108: 169–173, 2001.
14. **Florian JA, Kosky JR, Ainslie K, Pang Z, Dull RO, Tarbell JM.** Heparan sulfate proteoglycan is a mechanosensor on endothelial cells. *Circ Res* 93: e136–142, 2003.
15. **Gouverneur M, Spaan JA, Pannekoek H, Fontijn RD, Vink H.** Fluid shear stress stimulates incorporation of hyaluronan into endothelial cell glycocalyx. *Am J Physiol Heart Circ Physiol* 290: H458–H462, 2006.
16. **Hargens AR, Richardson S.** Cardiovascular adaptations, fluid shifts, and countermeasures related to space flight. *Respir Physiol Neurobiol* 169 *Suppl* 1: S30–33, 2009.
17. **Kang H, Fan Y, Deng X.** Vascular smooth muscle cell glycocalyx modulates shear-induced proliferation, migration, and NO production responses. *Am J Physiol Heart Circ Physiol* 300: H76–H83, 2011.
18. **Kang H, Sun L, Huang Y, Wang Z, Zhao P, Fan Y, Deng X.** Regional specific adaptation of the endothelial glycocalyx dimension in tail-suspended rats. *Pflugers Arch* 467: 1291–1301, 2015.
19. **Koo A, Dewey CF Jr, Garcia-Cardena G.** Hemodynamic shear stress characteristic of atherosclerosis-resistant regions promotes glycocalyx formation in cultured endothelial cells. *Am J Physiol Cell Physiol* 304: C137–C146, 2013.
20. **Li JP.** Glucuronyl C5-epimerase an enzyme converting glucuronic acid to iduronic acid in heparan sulfate/heparin biosynthesis. *Prog Mol Biol Transl Sci* 93: 59–78, 2010.
21. **Lin LJ, Gao F, Bai YG, Bao JX, Huang XF, Ma J, Zhang LF.** Contrasting effects of simulated microgravity with and without daily -Gx gravitation on structure and function of cerebral and mesenteric small arteries in rats. *J Appl Physiol (1985)* 107: 1710–1721, 2009.
22. **Ma J, Kahwaji CI, Ni Z, Vaziri ND, Purdy RE.** Effects of simulated microgravity on arterial nitric oxide synthase and nitrate and nitrite content. *J Appl Physiol (1985)* 94: 83–92, 2003.
23. **Ma J, Zhang LF, Yu ZB, Zhang LN.** Time course and reversibility of arterial vasoreactivity changes in simulated microgravity rats. *J Gravit Physiol* 4: P45–46, 1997.
24. **Megens RT, Reitsma S, Schiffers PH, Hilgers RH, De Mey JG, Slaaf DW, oude Egbrink MG, van Zandvoort MA.** Two-photon microscopy of vital murine elastic and muscular arteries. Combined structural and functional imaging with subcellular resolution. *J Vasc Res* 44: 87–98, 2007.
25. **Morey-Holton ER, Globus RK.** Hindlimb unloading rodent model: technical aspects. *J Appl Physiol (1985)* 92: 1367–1377, 2002.
26. **Musacchia XJ, Deavers DR, Meininger GA.** Fluid/electrolyte balance and cardiovascular responses: head-down tilted rats. *Physiologist* 33: S46–47, 1990.
27. **Musacchia XJ, Steffen JM, Fell RD, Dombrowski MJ.** Skeletal muscle response to spaceflight, whole body suspension, and recovery in rats. *J Appl Physiol (1985)* 69: 2248–2253, 1990.
28. **Nicogossian AE, Rummel JD, Leveton L, Teeter R.** Development of countermeasures for medical problems encountered in space flight. *Adv Space Res* 12: 329–337, 1992.
29. **Pahakis MY, Kosky JR, Dull RO, Tarbell JM.** The role of endothelial glycocalyx components in mechanotransduction of fluid shear stress. *Biochem Biophys Res Commun* 355: 228–233, 2007.
30. **Purdy RE, Duckles SP, Krause DN, Rubera KM, Sara D.** Effect of simulated microgravity on vascular contractility. *J Appl Physiol (1985)* 85: 1307–1315, 1998.
31. **Shi ZD, Abraham G, Tarbell JM.** Shear stress modulation of smooth muscle cell marker genes in 2-D and 3-D depends on mechanotransduction by heparan sulfate proteoglycans and ERK1/2. *PLoS One* 5: e12196, 2010.
32. **Shi ZD, Wang H, Tarbell JM.** Heparan sulfate proteoglycans mediate interstitial flow mechanotransduction regulating MMP-13 expression and cell motility via FAK-ERK in 3D collagen. *PLoS One* 6: e15956, 2011.
33. **Sides MB, Vernikos J, Convertino VA, Stepanek J, Tripp LD, Draeger J, Hargens AR, Kourtidou-Papadeli C, Pavy-LeTraon A, Russomano T, Wong JY, Buccello RR, Lee PH, Nangalia V, Saary MJ.** The Bellagio Report: Cardiovascular risks of spaceflight: implications for the future of space travel. *Aviat Space Environ Med* 76: 877–895, 2005.
34. **Sun LW, Wang C, Pu F, Li de Y, Niu HJ, Fan YB.** Comparative study on measured variables and sensitivity to bone microstructural changes induced by weightlessness between in vivo and ex vivo micro-CT scans. *Calcif Tissue Int* 88: 48–53, 2011.
35. **Uyama T, Kitagawa H, Tanaka J, Tamura J, Ogawa T, Sugahara K.** Molecular cloning and expression of a second chondroitin N-acetylgalactosaminyltransferase involved in the initiation and elongation of chondroitin/dermatan sulfate. *J Biol Chem* 278: 3072–3078, 2003.
36. **Wilkerson MK, Muller-Delp J, Colleran PN, Delp MD.** Effects of hindlimb unloading on rat cerebral, splenic, and mesenteric resistance artery morphology. *J Appl Physiol (1985)* 87: 2115–2121, 1999.
37. **Woodman CR, Schrage WG, Rush JW, Ray CA, Price EM, Hasser EM, Laughlin MH.** Hindlimb unweighting decreases endothelium-dependent dilation and eNOS expression in soleus not gastrocnemius. *J Appl Physiol (1985)* 91: 1091–1098, 2001.
38. **Xue JH, Chen LH, Zhao HZ, Pu YD, Feng HZ, Ma YG, Ma J, Chang YM, Zhang ZM, Xie MJ.** Differential regulation and recovery of intracellular Ca2+ in cerebral and small mesenteric arterial smooth muscle cells of simulated microgravity rat. *PLoS One* 6: e19775, 2011.
39. **Zhang LF.** Vascular adaptation to microgravity: what have we learned? *J Appl Physiol (1985)* 91: 2415–2430, 2001.
40. **Zhang LF, Ma J, Mao QW, Yu ZB.** Plasticity of arterial vasculature during simulated weightlessness and its possible role in the genesis of postflight orthostatic intolerance. *J Gravit Physiol* 4: P97–100, 1997.